THE ACS LCID PROJECT VII: THE BLUE STRAGGLERS POPULATION IN THE ISOLATED DSPH GALAXIES CETUS AND TUCANA[1]

M. Monelli[2,3], S. Cassisi[4], M. Mapelli[5], E.J. Bernard[6,2], A. Aparicio[2,3], E.D. Skillman[7], P.B. Stetson[8], C. Gallart[2,3], S.L. Hidalgo[2,3], L. Mayer[9,10], and E. Tolstoy[11]

Draft version September 30, 2011

ABSTRACT

We present the first investigation of the Blue Straggler star (BSS) population in two isolated dwarf spheroidal galaxies of the Local Group, Cetus and Tucana. Deep HST/ACS photometry allowed us to identify samples of 940 and 1214 candidates, respectively. The analysis of the star formation histories of the two galaxies suggests that both host a population of BSSs. Specifically, if the BSS candidates are interpreted as young main sequence stars, they do not conform to their galaxy's age-metallicity relationship. The analysis of the luminosity function and the radial distributions support this conclusion, and suggest a non-collisional mechanism for the BSS formation, from the evolution of primordial binaries. This scenario is also supported by the results of new dynamical simulations presented here. Both galaxies coincide with the relationship between the BSS frequency and the absolute visual magnitude M_V found by Momany et al. (2007). If this relationship is confirmed by larger sample, then it could be a valuable tool to discriminate between the presence of BSSs and galaxies hosting truly young populations.

Subject headings: (stars:) blue stragglers Local Group galaxies: individual (Cetus dSph, Tucana dSph) galaxies: evolution Galaxy: stellar content

1. INTRODUCTION

Blue Straggler stars (BSSs) were first identified in the Galactic globular cluster (GGC) M3 by Sandage (1953), as a group of stars bluer and brighter than the cluster turn-off stars, thus being more massive than the stars currently evolving at the turn-off (TO). Since then, BSSs have been identified in a variety of stellar systems in very different environmental conditions including: the field (Carney et al. 2005), open clusters (Liu et al. 2008), globular clusters (e.g., Piotto et al. 2004), and dwarf galaxies (Lee et al. 2003; Momany et al. 2007). Their puzzling position in the color-magnitude diagram (CMD) suggested

that they do not fit in the traditional scheme of stellar evolution for single stars. In fact, in order to populate that region of the CMD, these exotic objects must have experienced a physical process able to allow them to still stay in the core H-burning stage despite of their mass and the cluster age (for a detailed historical review, see Stryker 1993).

Presently, two different physical mechanisms are favored for explaining the formation of BSSs: *i)* coalescence through direct stellar collisions (COL-BS, Hills & Day 1976), and *ii)* evolution of primordial binary systems, in which mass transfer between the two components allows the rejuvenation of the secondary component (MT-BSS, McCrea 1964). It is also widely accepted that these two scenarios are not in competition, but they could both occur simultaneously in a stellar system. In fact, the coexistence of BSSs formed through both the collisional and mass transfer channels is commonly invoked to interpret the radial distribution of BSSs in many GGCs. The higher central concentration is explained by an efficient rate of stellar collisions in the densest regions, while the rise at large distance would be due to MT-BSSs (Mapelli et al. 2006; Ferraro et al. 2009) surviving in the outskirts.

While the scenario for BSSs in Galactic clusters is well settled, at least from the observational point of view, in contrast, this is not true for dwarf galaxies. In fact, even though the first indication for the presence of BSS candidates in the Sextans dwarf dates back to Mateo et al. (1991), and, since then, several observational findings suggest the presence of BSS candidates in several dSphs (see, e.g., Mapelli et al. 2009, and references therein), we are still faced with the problem of understanding if these candidates are *genuine* BSSs or *normal* core H-burning stars belonging to an, albeit sparse, intermediate-age stellar population.

[1] Based on observations made with the NASA/ESA *Hubble Space Telescope*, obtained at the Space Telescope Science Institute, which is operated by the Association of Universities for Research in Astronomy, Inc., under NASA contract NAS5-26555. These observations are associated with program 10505.
[2] Instituto de Astrofísica de Canarias, La Laguna, Tenerife, Spain; monelli@iac.es, carme@iac.es, antapaj@iac.es, shidalgo@iac.es.
[3] Departamento de Astrofísica, Universidad de La Laguna, Tenerife, Spain
[4] INAF-Osservatorio Astronomico di Collurania, Teramo, Italy; cassisi@oa-teramo.inaf.it.
[5] Università di Milano Bicocca, Dipartimento di Fisica G.Occhialini, Piazza della Scienza 3, I–20126, Milano, Italy; mapelli@mib.infn.it
[6] Institute for Astronomy, University of Edinburgh, Royal Observatory, Blackford Hill, Edinburgh EH9 3HJ, UK; ejb@roe.ac.uk
[7] Department of Astronomy, University of Minnesota, Minneapolis, USA; skillman@astro.umn.edu.
[8] Dominion Astrophysical Observatory, Herzberg Institute of Astrophysics, National Research Council, Victoria, Canada; peter.stetson@nrc-cnrc.gc.ca.
[9] Department of Physics, Institut für Astronomie, ETH Zürich, Zürich, Switzerland; lucio@phys.ethz.ch.
[10] Institut für Theoretische Physik, University of Zurich, Zürich, Switzerland; lucio@physik.unizh.ch.
[11] Kapteyn Astronomical Institute, University of Groningen, Groningen, Netherlands; etolstoy@astro.rug.nl.

TABLE 1
The distance modulus, reddening, and candidate BSS
properties.

—	Cetus	Tucana
$(m-M)_0$	24.46 ± 0.12	24.74 ± 0.12
$E(B-V)$	0.028	0.031
$N_{BS}{}^a$	940	1214
$N_{BS_{evol}}{}^b$	90	123
$F_{BS}{}^c$	0.05 ± 0.05	0.02 ± 0.04
N_{AC}^d	3	6

^{a} Number of candidate BSSs
^{b} Number of evolved BSSs in the core He-burning stage
^{c} Logarithmic frequency of BSSs with respect HB of stars
^{d} Number of Anomalous Cepheids

Recently, a few studies have focused on the properties of BSSs in nearby dSph galaxies in the Local Group (LG). Mapelli et al. (2007) presented wide field data for the galaxies Draco and Ursa Minor, concluding that the population of BSSs is, in both systems, compatible with the MT-BSS scenario. Mapelli et al. (2009) discussed the properties of BSSs in Sculptor and Fornax. Sculptor presents similarities with both Draco and Ursa Minor, as its BSS population is also compatible with a MT-BSS population. On the contrary, the relatively strong central radial concentration of the BSS candidate stars in Fornax favors the presence of an intermediate-age stellar population (in agreement with previous studies of the star formation history (SFH) of Fornax).

Unraveling the nature of the BSS candidates has important implications for our understanding of the SFHs of these galaxies. For example, whenever it is possible to discriminate between a sequence of BSSs and a young MS population, it is possible to set a constraint on the age of the last star formation event in a galaxy. Therefore, the BSS populations in Draco, Ursa Minor, and Sculptor suggest that no star formation occurred in the last few Gyr in these galaxies.

Intriguingly, Momany et al. (2007) found a statistically significant anti-correlation between the frequency of BSSs and the absolute visual magnitude (M_V) of 8 nearby dSphs. The anti-correlation is valid over a large range of luminosities, and presents a different slope than that of GGCs. In addition, Momany et al. (2007) ruled out the possibility that collisional binaries could have contributed to the observed BSS populations and concluded that the BSSs in dwarf spheroidal galaxies are mainly formed via mass exchange in primordial binaries.

In view of the important implications of the presence of a sizable sample of BSSs in a dwarf galaxy, it is worthwhile to apply the approach outlined by Momany et al. (2007) to other dwarfs. The hope is to eventually produce independent constraints useful for addressing the true nature of the BSS candidates.

In this paper, we investigate these issues further by analyzing the properties of candidate BSSs in the isolated dSphs Cetus and Tucana. The data sets are part of the LCID project (*Local Cosmology from Isolated Dwarfs*), aimed at recovering the full SFHs of six isolated LG galaxies: Cetus and Tucana (dSph), LGS 3 and Phoenix (dIrr/dSph), IC 1613 and Leo A (dIrr). The plan of the paper is as follows: in the next section we briefly describe
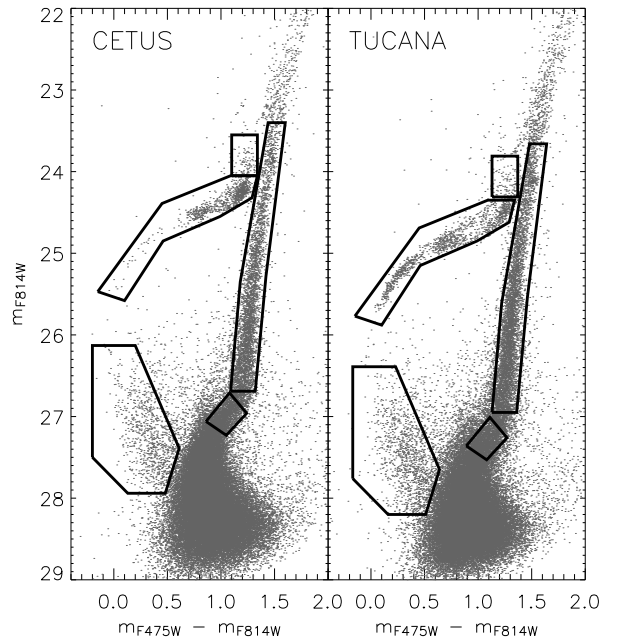

Fig. 1.— The observed CMDs for the two dwarfs: Cetus (left panel) and Tucana (right panel). The delimited areas represent the regions of the CMDs selected for the present analysis (see the text for more details).

the photometric data set and outline the criteria for selecting the candidate BSSs in the observed CMDs. In §3 we investigate the properties of the BSS populations. §4 presents the results of dynamical simulations. The discussion and final remarks close the paper.

2. THE OBSERVATIONS AND THE SELECTION OF SAMPLES

The observations used in this paper have already been presented in Monelli et al. (2010b, Cetus) and Monelli et al. (2010c, Tucana). Here we summarize the main points relevant to the following discussion. The images were collected with the ACS camera aboard the HST, under the project *The onset of star formation in the universe: constraints from nearby isolated dwarf galaxies* (PID 10505, PI C. Gallart). A total of 25 and 32 orbits have been devoted to Cetus and Tucana, respectively, using the $F475W$ and $F814W$ filter pass bands. The photometric reduction has been performed using the DAOPHOT/ALLFRAME package (Stetson 1994). The final catalog has been calibrated to the VEGAMAG system using the transformations presented in Sirianni et al. (2005). The adopted distance modulus and reddening are summarized in Table 1, together with other quantities calculated in this work.

Figure 1 shows the CMDs of the two galaxies, with the regions adopted to select the various samples studied superimposed. Note that we adopted the same boxes for both galaxies, applying a shift to take into account the differences in distance modulus and reddening. The CMDs of both galaxies are ≈ 1.5 mag deeper than the TO, reaching $m_{F814W} \sim 28.8$ mag. The blue plume of candidate BSSs emerges clearly in the CMD, for $m_{F475W} - m_{F814W} < 0.5$ mag, $26 \lesssim m_{F814W} \lesssim 28$.

We defined a box in this region to include the bulk of these stars. Note that there are a number of objects between the BSSs region and the red giant branch (RGB). We decided not to include these stars for two reasons: *i)* it is possible that blended objects from the most populated TO region are polluting this part of the CMD; *ii)* in this color range, we expect to find stars evolved off the main sequence. Also, we did not include the brightest objects ($m_{F814W} \sim 26.2$) because it is possible that they are extreme horizontal branch (HB) stars. Also note that we estimated a negligible contamination from both foreground Galactic stars (due both to the small area covered and the high Galactic latitude of the two galaxies) and background galaxies (thanks to the careful cleaning of the catalogs, see Monelli et al. 2010b). Figure 1 also shows the regions adopted to select stars in the HB, the RGB, and the progeny of BSSs during the central helium burning phase. This last box has been placed above the red HB, paying attention not to include the AGB clump, which clearly appears in the CMDs of both galaxies ($m_{F814W} \sim 23.4$ mag).

3. ANALYSIS OF THE CANDIDATE BSS

In the box covering the blue plume, we have identified 940 and 1214 objects in Cetus and Tucana, respectively, which we consider as BSS candidates. Note that the present data cover a significant fraction of the body of Tucana (tidal radius $r_t = 3.45'$), which was centered in the ACS field (field-of-view 3.4′). However, Cetus occupies a larger area in the sky ($r_t \sim 32'$, McConnachie & Irwin 2006[12]), and the sampled field covers a smaller fraction. Moreover, the observed field was offset from the center so that the innermost regions of Cetus were not observed (Monelli et al. 2010b). If we take this into account, following the reasoning of Bernard et al. (2009) to estimate the total number of RR Lyrae stars, the total number of BSS candidates in Cetus is estimated to be $\simeq$ 5,000 stars.

The most important question is to assess the nature of these stars. BSSs have been found in very different environments, from the field, to low-density stellar systems such as open clusters and dwarf spheroidals, and in most globular clusters. They are therefore common products, and it is reasonable to expect to find them in Tucana and Cetus as well. Therefore, the basic question we are trying to address is: are these candidates genuine BSSs, or is there also a significant component of truly young stars? In the following sections we will try to address this using different observables.

3.1. *Clues from the detailed SFH analysis*

The main objective of the LCID project was to derive accurate SFHs for a sample of six isolated galaxies in the Local Group, in order to understand their evolution in a cosmological context. To do this, we adopted well-established techniques based on the comparison of the observed CMD with a synthetic one. We devoted significant effort to investigating the error budget and also possible systematics affecting our solution, due to the use

of different photometric packages, stellar evolutions libraries, SFH codes. The main conclusion (see Monelli et al. 2010b,c; Hidalgo et al. 2011) of this analysis was that we can rely, within the error bars, on both the uniqueness and stability of the derived solutions. Therefore, the most important features recovered, such as the epoch and the duration of the main star formation events, including those at the oldest epoch, and the age-metallicity relations are solid results.

The SFHs presented in Monelli et al. (2010b) and Monelli et al. (2010c), for Cetus and Tucana respectively, show that both galaxies are made of old and metal-poor populations. In particular, both galaxies formed 90% of their stars at epochs older than 9 Gyr ago, and the bulk of the stars have metallicities in the range $0.0001 < Z < 0.001$. In addition, both galaxies present a well defined age-metallicity relation in the sense of increasing metallicity with decreasing age.

The SFH reconstructions indicate a small population ($< 3\%$ in mass) of stars significantly younger than the majority of stars ($2 < t < 5$ Gyr) but with metallicities consistent with the oldest stars ($Z < 0.0006$). Thus, these stars do not follow the general age-metallicity relations in these two galaxies. The analysis of the best-fit CMDs show that they nicely populate the blue plume region of the CMD, brighter and bluer than the oldest MS turn-off. The possibility that the metallicity of these stars has been understimated by the code is excluded with high confidence level. In fact, higher metallicity and an age of ≈ 4 Gyr, would produce also a redder RGB sequence that is not observed. On the basis of the retrieved SFH, Monelli et al. (2010b) made the hypothesis that the sequence of blue stars, brighter than the old MS Turn-Off, are consistent with a population of BSSs, characterized by the same metal content as the metal-poor dominant stellar component.

An alternative interpretation would be that these are truly young metal-poor MS stars, formed as a consequence of gas accretion. However, it seems very unlikely that two galaxies, that spent most of their life in isolation, accreted gas and formed stars of the same metallicity and at the same epoch, in one event that created roughly the same amount of mass (3% of the total stellar mass).

3.2. *Comparison with stellar evolutionary models*

Figure 2 shows the comparison of the Tucana CMD with theoretical tracks from the BaSTI database[13] of stellar evolution models (Pietrinferni et al. 2004). Here we note that the analysis of the SFH for the LCID galaxies has been performed by using the same evolutionary framework; so the present analysis is fully consistent with those concerning the SFHs. The selected tracks span the range of metallicities suggested by the SFHs, Z = 0.0001, 0.0003, 0.0006, and 0.001 as an upper limit.

The figure discloses some interesting clues. First, the black lines in the left panel show the Zero Age Main Sequence (ZAMS) for two metallicities: Z=0.0001 (solid line) and Z = 0.001 (dashed). The comparison with the observed CMDs shows that both ZAMSs border the blue envelope of the BSS sequence, independent of the assumed metal content. Moreover, the same panel shows

---

[12] New preliminary estimates based on wide-field Subaru data confirm values $r_t > 15'$ (Bernard et al, 2012, in prep.), therefore significantly larger than the ACS field-of-view.

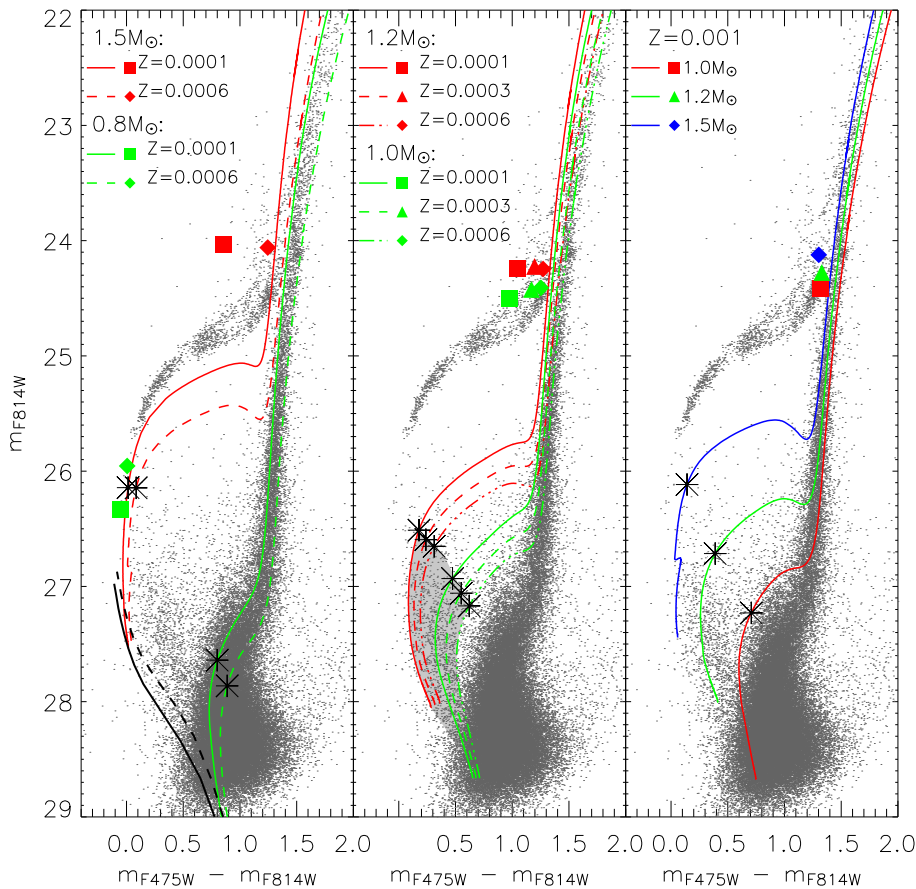[13] *http://www.oa-teramo.inaf.it/BASTI*

FIG. 2.— The CMD of Tucana with superimposed a selected sample of evolutionary stellar models for the labeled assumptions about the initial stellar mass and chemical compositions. Note that, to avoid confusion, the tracks are plotted until the tip of the RGB, and that the filled symbols mark the Helium ignition. We have adopted the values of distance modulus and reddening, from Bernard et al. (2008), as summarized in Table 1. *Left* - The 1.5 and $0.8M_\odot$ bracket the entire sequence of candidate BSSs. The two black lines show the ZAMS for metallicity z=0.0001 (solid) and Z=0.001 (dashed), which outline the blue edge of the sequence. *Central* - We show the ranking with metallicity of stars of 1.0 (green) and 1.2 (red) $M_\odot$. The shaded area encloses the central hydrogen burning phase, until the exhaustion marked by the asterisks. *Right* - Comparison with models with fixed metallicity (Z=0.001) and three different masses (1.0, 1.2, 1.5 $M_\odot$).

that the maximum mass fitting the brightest objects is equal to about 1.5 $M_\odot$ (red lines), again with a negligible dependence on the assumed metallicity (Z=0.0001, 0.001 for the red solid and dashed lines, respectively). The same figure also shows the location of two theoretical tracks corresponding to $0.8M_\odot$ stellar models (green lines), taken as representative of the stellar structures currently evolving at the TO and sub-giant branch of both galaxies. The filled symbols show the first point corresponding to the central helium burning phase. It is evident - as also fully supported by the SFH analysis - that for the TO and the SGB, a range of metallicities in the adopted evolutionary framework is required to properly interpret the observed morphology of the CMD. This comparison reveals that the maximum mass of the stars in the blue plume is at most ~ 2 times larger than the mass of the stars at the TO. This occurrence is in good agreement with the properties of BSSs in other stellar

systems such as GGCs (see, i.e., Gilliland et al. 1998, and references therein).

The central panel shows the comparison with stellar tracks for different masses ($M = 1.0, 1.2M_\odot$, green and red lines, respectively), and different metallicities ($Z = 0.0001$-solid, $Z = 0.0003$-dashed, $Z = 0.0006$-dot-dashed). The shaded area encloses the region corresponding to the central hydrogen burning phase, whose end is marked by the asterisks. The bulk of BSS candidates clearly occupies this region of the CMD.[14] The plot clearly shows that a spread in mass is needed to fit the observed distribution of blue plume stars. A spread in metallicity is also possible but, as shown in the right

[14] Although the adopted stellar models are obtained in the canonical evolutionary framework, i.e., they do not account for the physical processes at the basis of BSS formation, we think that in order to have a rough estimate of the metallicity range spanned by the BSS candidates, they are still suitable.
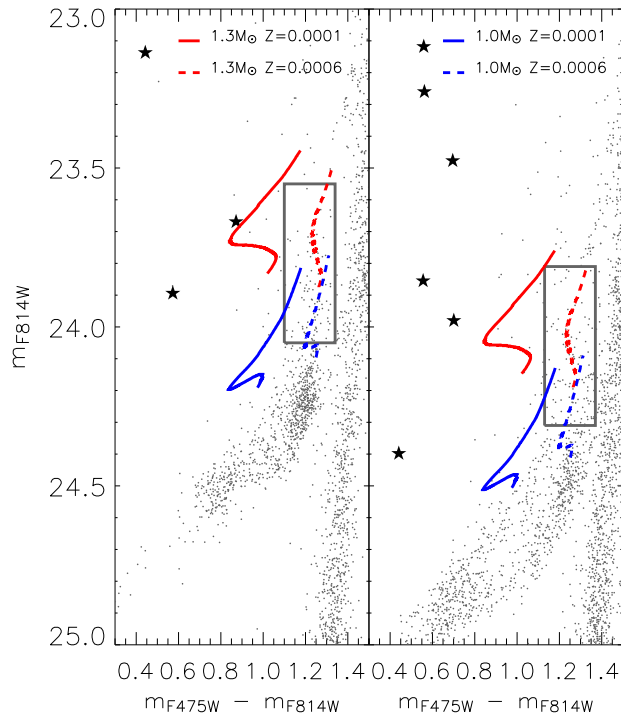
FIG. 3.— Similar to Figure. 2, but we present a zoom of the CMD of Cetus (left panel) and Tucana (right panel), corresponding to the core He-burning stage. In each panel the box represents the region used to select the candidate progeny of the blue plume stars. Four tracks are overplotted, for different mass and metallicity assumptions. The filled stars mark the location of the anomalous Cepheid variables detected in these galaxies (Bernard et al. 2009).

panel of the same figure, values larger than $Z > 0.001$ seem unlikely. The 1.0 $M_\odot$ track is too faint and too red to represent the bulk of the blue plume objects. The 1.2 $M_\odot$ still gives a good representation, and can be considered as an upper limit both in term in of mass and metallicity. In fact, despite the 1.5 $M_\odot$ still limits the brightest blue plume stars, the age of this model at the turn-off ($\sim$1.3Gyr) is in contrast with the finding of the SFH. On the other hand, higher metallicities would shift the tracks to redder color and fainter magnitude, significantly worsening the agreement in particular in the RGB phase. Thus, relatively metal-poor and relatively massive ($> 1\ M_\odot$) stellar structures are preferred to better represent the peak of the distribution. Therefore, the metallicity derived for the BSS candidates is in good agreement with that estimated for the bulk of the older populations, as discussed in §3.1, and not in agreement with the higher metallicities found at the end of the initial episodes of star formation in Cetus and Tucana. This result can be considered a circumstantial evidence supporting the idea that - at least a large fraction of - the stars located along the blue plume could be genuine BSSs; in fact if they were true young stars formed in a late star formation burst, they would have a metallicity lower than that one could expect of the basis of a standard age-metallicity relation.

Additional information can be provided by the study of the BSS progeny in the core He-burning stage. Evolutionary models for MS stars predict that stars more massive than about 1$M_\odot$ are located in the red side of the HB at a magnitude level depending on their He core

mass (Castellani & Degl'Innocenti 1995). In particular, the right-hand panel of Figure 2 suggests that the evolved stars in this mass range all clump in the same region of the CMD. This implies that the progeny of BSSs of similar mass, independent of the formation mechanism (see, e.g., Sills et al. 2009), should occupy a similar region in the CMD, redder and brighter than their low-mass counterparts. This means that, on the one hand, the distribution of BSS progeny in the CMD provides very little information about the mass distribution of the BSS population above 1$M_\odot$. On the other hand, the ratio of the number of stars can be compared with theoretical expectations based on the evolutionary lifetimes in the core H- and He-burning stages.

Figure 3 shows an expanded view of the HB region of the Cetus (left panel) and Tucana (right panel) CMDs. Superimposed to both plots are the evolutionary tracks, starting with the onset of the central helium burning, for two masses (1.0 -blue line- and 1.3 -red-$M_\odot$) and two metallicities ($Z = 0.0001$ -solid- and $Z = 0.0006$ -dashed-). The boxes corresponding to our selections are shown. Both panels show the presence of a sparse sequence above the red HB. While a few of them, which are located close to theoretical prediction for the most metal-poor stars, fall outside our box, the majority of stars, inside the box, look more compatible with slightly more metal-rich tracks. Note that this is in agreement with the SFH results, which gives for the two galaxies a mean metallicity of the order of $Z = 0.0004$ (Cetus) and $Z = 0.0006$ (Tucana).

To further investigate the interpretation that the stars located inside the box showed in Fig. 3 can be really considered the progeny of the stars located along the MS blue plume, we compared the star counts ratio between the objects located inside the two boxes with theoretical predictions obtained taking into the account the information from the SFH. Monelli et al. (2010b, their Fig 18) have already shown a synthetic CMD built from the SFH solution of Cetus, where stars with colors and magnitudes typical of a population of BSSs clearly appear. We therefore counted the stars using the same boxes defined here, and estimated the same ratio using a best-fit CMD for both Cetus and Tucana. The derived ratios are 0.08±0.01 and 0.08±0.01 for Cetus and Tucana respectively. Analogous estimates can be made from the observed CMD. The number of BSSs in Cetus and Tucana are 940 and 1214, respectively, while the number of objects in the evolved phase are 90 and 123. This gives ratios of 0.10±0.01 for Cetus and 0.10±0.01 for Tucana. This shows that there is good agreement with the empirical values. This suggests that the selected stars are the evolved counterpart of blue plume objects. Moreover, this test strongly suggests that, if we are dealing with a pure BSSs population, the analysis performed using models calculated for normal MS stars is only marginally affecting the results.

It is also worth noting that the progeny of BSS - in particular the more massive ones - can cross the instability strip for radial pulsation during the core He-burning stage; in this case they pulsate as anomalous Cepheids (Bono et al. 1997). When studying the populations of variable stars in the LCID galaxies, Bernard et al. (2009) discovered three anomalous Cepheids in Cetus, and six in Tucana. The locations of these variable stars in the
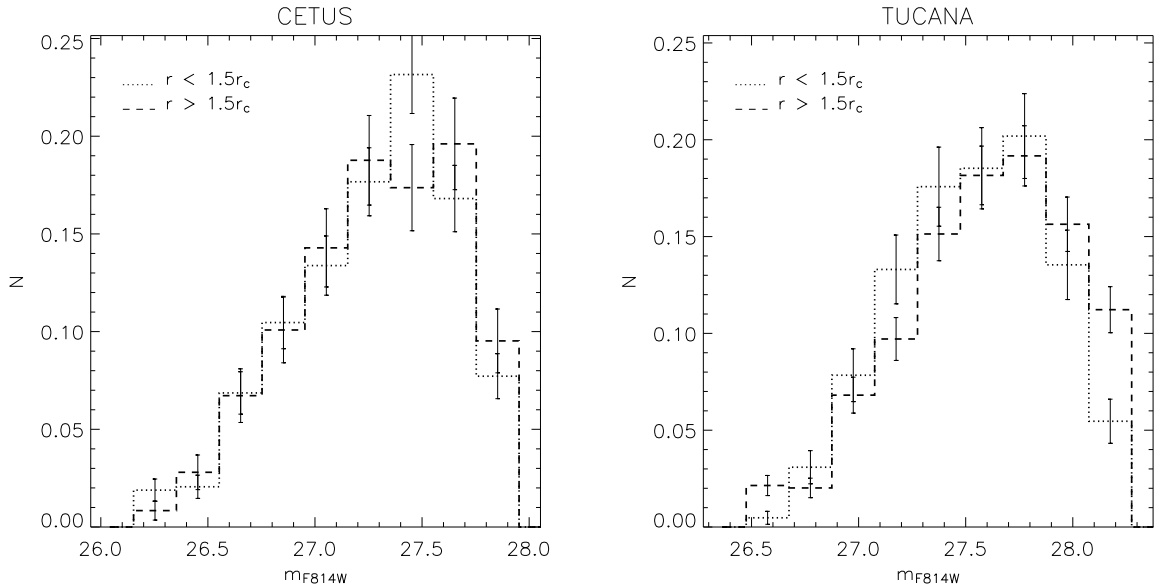
Fig. 4.— Normalized luminosity function of the candidate BSS population in Cetus (left panel) and Tucana (right panel). The different lines refer to the BSS stars within (dotted) and outside (dashed) $1.5r_c$ from the center.
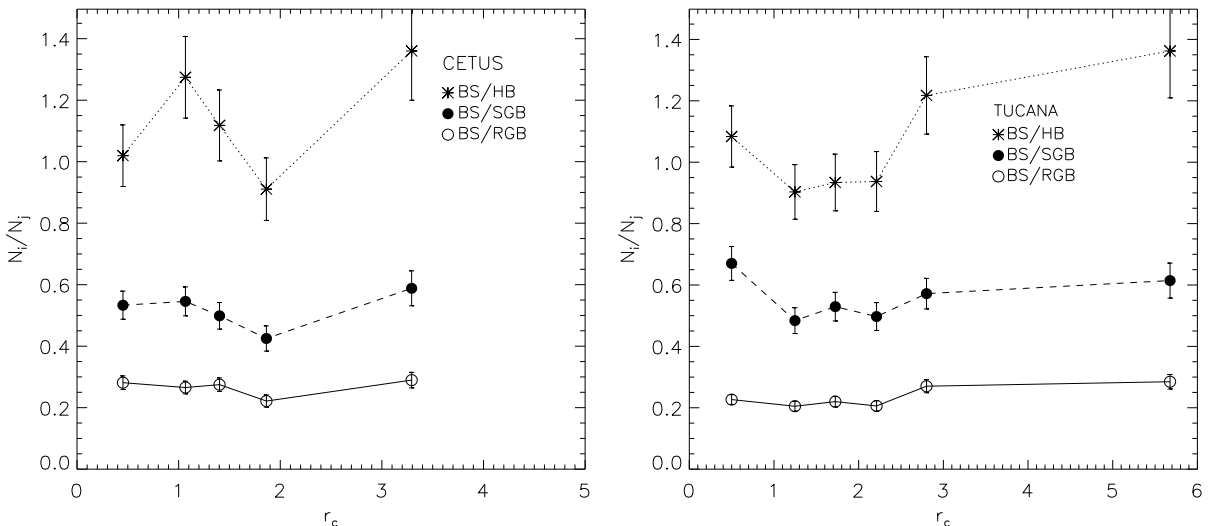

Fig. 5.— Ratios of the number of BSSs with respect of HB (asterisks), SGB (full circles), and RGB (open circles) stars, as a function of the galactocentric radius for Cetus (left) and Tucana (right).

CMDs of both galaxies are shown in Fig. 3. They appear bluer and brighter than the expected bulk of the BSS progeny. This suggests that anomalous Cepheids might have slightly larger masses than the typical BSS.

3.3. Luminosity function

The luminosity function of blue plume stars is a powerful diagnostic to both infer information on their nature and, in case of a BSS population, to distinguish between the two main formation mechanisms. In fact, if these stars belong to an intermediate-age population, we expect to find them more centrally concentrated (see next section) and also that the brightest (youngest) are preferentially located to the innermost regions. On the other hand, it has been found that in GGCs the BSS luminosity function changes as a function of radial distance (Monkman et al. 2006), in the sense that the brightest

BSS stars are preferentially located in the central regions. Since there is no doubt that in GC we only have BSSs, with no contamination from intermediate-age stars, this occurrence is explained with a combination of two different formation mechanisms. Collisions, which are efficient in the inner regions of GGC, tend to create bluer and brighter BSSs (Bailyn & Pinsonneault 1995; Bailyn 1995). In the outer parts of the GGCs, the BSSs are predominantly created from primordial binaries. In dSph galaxies the formation of COL-BSS is highly disfavored due to the very low stellar density, so that we do not expect to observe a similar behavior (Mapelli et al. 2007; Momany et al. 2007). Therefore, in case a central concentration of the brightest blue plume stars were observed, this would point to the presence of a genuine intermediate-age population.
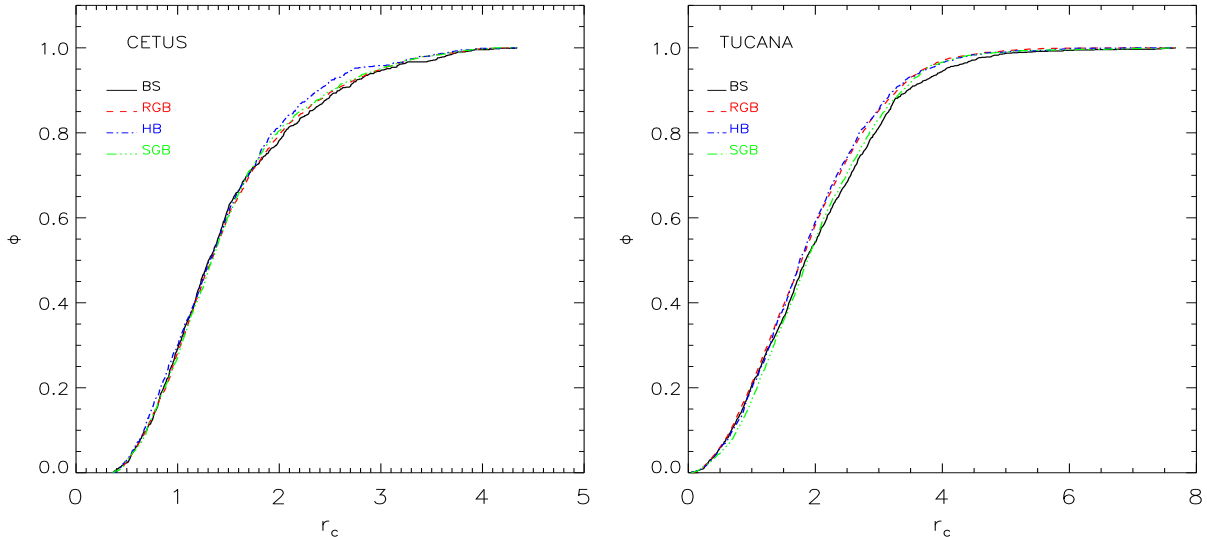
FIG. 6.— Normalized cumulative distributions for the samples of BSSs (black solid line), RGB (red dashed), HB (blue dot-dashed), and SGB (green) stars for Cetus (left panel) and Tucana (right).

Figure 4 shows the BSS candidates luminosity function for Cetus (left panel) and Tucana (right panel). The plot shows the luminosity function of stars inside (dotted line) and outside (dashed line) a distance of 1.5 times the core radius, r_c. Due to the different number of stars and area covered by the two samples, the curves were normalized to their area. The shape of the luminosity function does not change significantly as a function of radius, and similarly we do not find any evidence for an obvious shift in the magnitude of the peak.

We find that the fraction of the brightest BSSs (BS^{br}, i.e., within 0.5 mag of the brightest), is also constant with radius. For the inner and outer regions we found $N(BS^{br})/N(BS) = 0.12 \pm 0.02$ and 0.12 ± 0.03 in the case of Cetus, and $N(BS^{br})/N(BS) = 0.12 \pm 0.03$ and 0.13 ± 0.02 for Tucana. Note that the errors are solely Poisson statistical errors.

Thus, we find no evidence for segregation in either galaxy, supporting the absence of centrally concentrated bright stars, and supporting that the population of BSSs in Cetus and Tucana is formed as a result of the evolution of binary systems, even in the innermost regions.

3.4. Radial distribution

This last result can be further verified studying the radial distribution of candidate BSSs compared to that of other stellar tracers. It has been found in many GGCs that the radial profile of BSSs has a central cusp (c.f., Bailyn 1995), which falls to a minimum (the 'zone of avoidance' Mapelli et al. 2004), and then increases with radius. This phenomenon has again been interpreted with the different formation mechanisms at work: the COL-BSSs are more centrally concentrated than MT-BSS (Bailyn & Pinsonneault 1995), which instead dominate in the outskirts of clusters. If COL-BSSs are not present in dSphs, we expect no central concentration, as verified by Mapelli et al. (2007) and Mapelli et al. (2009) for Draco, Ursa Minor and Sculptor.

Figure 5 presents the ratios $N_{BS\_HB} = N_{BS}/N_{HB}$, $N_{BS\_RGB} = N_{BS}/N_{RGB}$, and $N_{BS\_SGB} = N_{BS}/N_{SGB}$

for Cetus (left) and Tucana (right), as a function of the galactocentric distance expressed in units of core radius. We divided the complete catalog into five (Cetus) and six (Tucana) radial bins, containing the same total number of stars, according to the position of stars in elliptical annuli. The points in Figure 5 show the ratio in each elliptical radius, plotted as a function of the mean galactocentric distance of each annulus.

Figure 5 clearly shows the absence of strong central concentrations of BSSs in both galaxies. We tested the hypothesis that the ratios of the various samples are consistent with a flat distribution by comparing the ratios to the mean of the observed distribution. In the case of Cetus, we estimated non-reduced χ^2 of 6.6, 7.3, 9.3 for N_{BS_RGB}, N_{BS_SGB}, and N_{BS_HB}, respectively. The null hypothesis therefore has corresponding probabilities of 0.15, 0.12, and 0.05. This suggests that N_{BS_RGB} and N_{BS_SGB} are consistent with a flat distribution, while N_{BS_HB} is only marginally consistent. In the case of Tucana, we derive χ^2 values of 14.8, 10.6, 12.8 (N_{BS_RGB}, N_{BS_SGB}, N_{BS_HB}), corresponding to probabilities of 0.01, 0.06, and 0.03. This means that N_{BS_RGB} and N_{BS_HB} are not consistent with a flat distribution, while N_{BS_SGB} is only marginally consistent.

Although N_{BS_HB} has larger uncertainties than the other ratios, it is interesting to note that, qualitatively, N_{BS_HB} shows larger fluctuations than the others. Moreover, in the range $0 < r_c < 2$ the trend for the two galaxies is opposite. Cetus presents an initial increase followed by a drop, while in Tucana an initial decrease within the core radius is followed by the increase in the ratio of BSSs relative to HB stars. At large distance, there is mild evidence of an increase of N_{BS_HB}, especially for Tucana where the field covers a large area in terms of r_c. This is in agreement with the predictions by Mapelli et al. (2006).

Another way to represent the radial distribution of different samples is to use the cumulative distributions, shown in Figure 6 for the BSS, RGB, SGB, and HB stars. A Kolmogorov-Smirnov test gives probabilities of 0.861
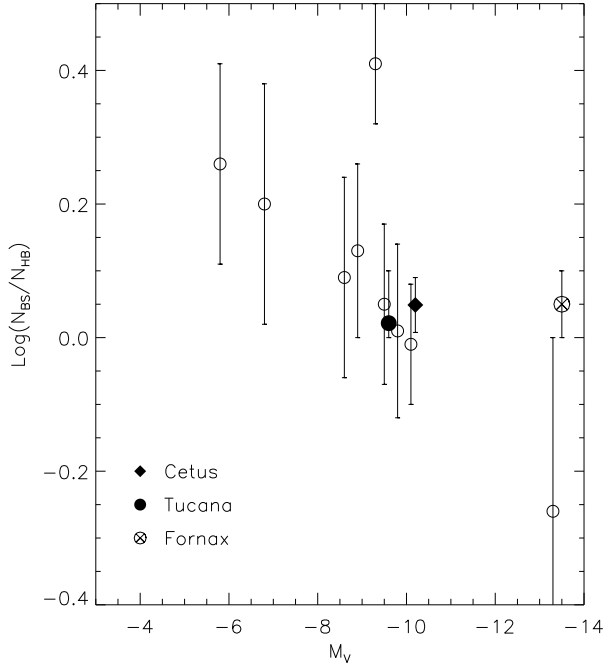
FIG. 7.— The logarithmic frequency of BSSs in Tucana (black circle) and Cetus (black diamond) as a function of the absolute visual magnitude. We also show the data corresponding to other LG dwarfs as obtained from Momany et al. (2007), and Fornax (crossed circle, Del Pino et al, 2011, in prep.).

(0.004), 0.48 (0.02), and 0.58 (0.28) for Cetus (Tucana) that the BSSs and the RGB/HB/SGB samples are drawn from the same parent population.

However, it is interesting to note that, starting from $3\, r_c$, the BSS cumulative distribution is systematically lower, in both galaxies, than the others. This indicates higher BSS frequencies at larger distances.

3.5. *Frequency versus M_V*

Momany et al. (2007) found that a linear correlation exists between the logarithmic frequency of BSSs (F_{BS}, normalized to the number of HB stars) and the absolute visual magnitude of nearby LG dwarfs. Interestingly enough, they found that this correlation is verified over a large range of **magnitudes**, and that its slope is significantly different, i.e., less steep, than a similar relation found by Piotto et al. (2004) for GGCs. Presently, an underlying physical mechanism for this trend has not been identified. Based on the selections presented in Figure 1, we estimated that F_{BS} is equal to 0.05±0.05 and 0.02±0.04 for Cetus and Tucana, respectively.

In Figure 7, these values are plotted together with data from other galaxies given in Figure 2 of Momany et al. (2007). We adopted the absolute M_V magnitude from McConnachie & Irwin (2006) for Cetus (−10.1 mag) and from Saviane et al. (1996) for Tucana (−9.6 mag). Fig. 7 shows that Tucana and Cetus are consistent with the relationship derived from other LG dwarfs. Using the analytic relation for F_{BS} from Momany et al. (2007), we obtain −0.01±0.08 and 0.03±0.08 for Cetus and Tucana, respectively, again, showing very good agreement with the observed values.

If we accept that the $F_{BS} - M_V$ relation is signifi-

cant, then this is an independent indication that the we are dealing with a genuine BSS population. If the blue plume stars were due to fluctuations in the SFH producing younger stars, one would not expect any relationship between F_{BS} and M_V. On the other hand, if blue plume stars are BSSs, they essentialy belong to the same population generating the HB stars. As already noted by Momany et al. (2007), the trend is similar in the case of globular clusters, but with significantly shallower slope. The existence of an anti-correlation with the luminosity (**the higher the luminosity, the lower the BSS frequency**), and hence with the mass of the cluster, might suggest that in more massive globular clusters the mechanisms affecting the binary systems are more efficient then in less massive ones, and this cause a deficiency of BSS with respect of HB stars (see Piotto et al. 2004). In dSph, the shallower slope might indicate that the same mechanisms are still at work, but are less efficient due to the lower density of dwarf galaxies.

On the basis of present results, it appears evident that if the reliability of $F_{BS} - M_V$ relation was confirmed by increasing the number of LG dwarfs in the sample, it could represent a valuable tool for discriminating stellar systems hosting truly young MS stars from those with a significant population of old, genuine BSSs. For example, a preliminary analysis of a deep CMD of Fornax dSph (Del Pino et al. 2011, in preparation, also shown in Figure 7 as a crossed-circle symbol) suggests that the F_{BS} estimate for this galaxy ($F_{BS} > 0.05±0.05$) is significantly higher than expected from its absolute magnitude ($F_{BS} = -0.23±0.08$). This is in agreement with the conclusion presented in Mapelli et al. (2009), and with the fact that Fornax hosts a population as young as 100 Myr (see also Stetson et al. 1998).

4. DYNAMICAL SIMULATIONS

Further clues about the origin of BSSs can be inferred from their dynamical evolution (see, e.g., Sigurdsson et al. 1994). We thus perform a wide sample of dynamical simulations, following the evolution of MT-BSS and COL-BSS populations in the potential of Cetus and Tucana.

4.1. *Method*

We use the code BEV (Sigurdsson & Phinney 1995), in the upgraded version described by Mapelli et al. (2004, 2006). The same code has been used to model BSSs in Draco, Ursa Minor (Mapelli et al. 2007), Sculptor and Fornax (Mapelli et al. 2009). BEV integrates the dynamical evolution of BSSs under the influence of the host-galaxy potential, dynamical friction, distant encounters with other stars, and three-body encounters (which are negligible for dSphs). The potential of the host galaxy is assumed to be time-independent and is represented by a multi-mass King model. The classes of mass are the same as in Mapelli et al. (2007), and the TO mass is assumed to be 0.8 $M_\odot$ (see Figure 2) for both Cetus and Tucana. To calculate the potential, we input the number density of stars in the core ($n_c = 0.03$ and = 0.12 stars pc^{-3} for Cetus and Tucana, respectively) the velocity dispersion in the core (we assume $\sigma_c = 10$ km s^{-1} for both Cetus
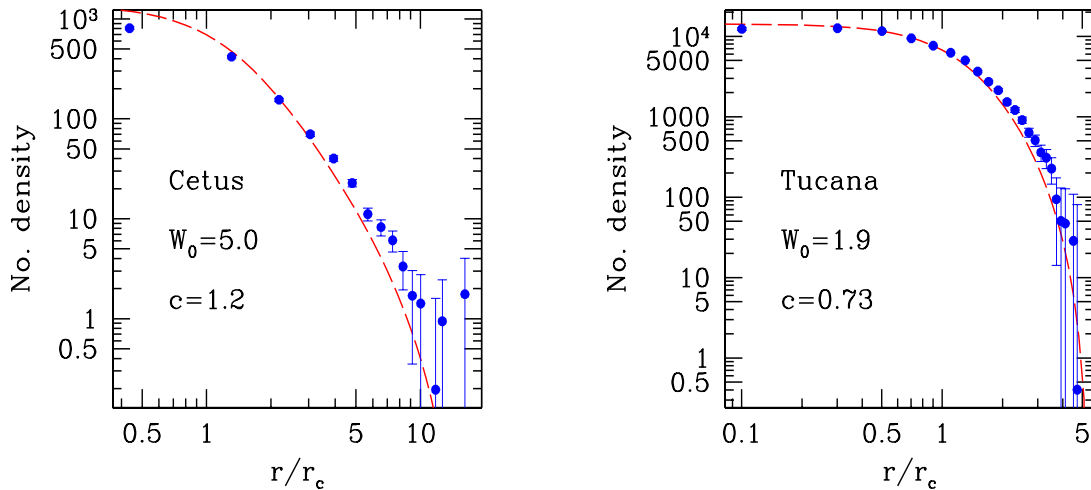
FIG. 8.— Simulated stellar radial profile (dashed line, red on the web) for Cetus (left-hand panel) and Tucana (right-hand panel), compared with observations (filled circles, blue on the web). The number density is given in stars per square arcmin. Data points for Cetus are based on deep Subaru data (Bernard et al. 2011, in prep.), while are taken from Bernard et al. (2009) for Tucana.
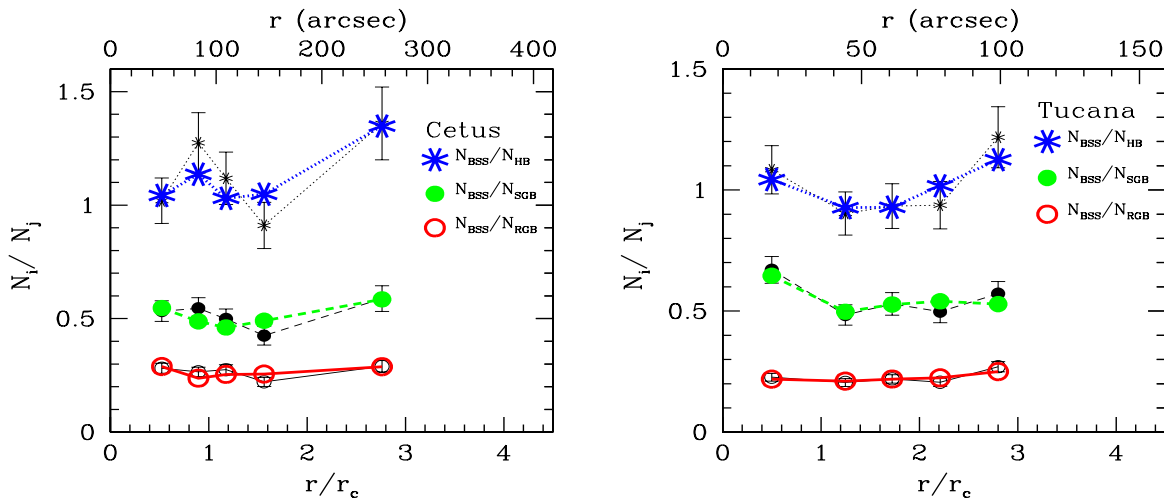

FIG. 9.— Simulated radial distribution of $N_{\rm BS\_RGB}$, $N_{\rm BS\_SGB}$ and $N_{\rm BS\_HB}$ in Cetus (left-hand panel) and in Tucana (right-hand panel). Thin lines indicate the observed radial distributions, for comparison with the best match simulations (runs C3 and T3 for Cetus and Tucana, respectively). Error bars account for Poisson uncertainties.

and Tucana[15]), and we modify the central adimensional potential W_0 (defined in Sigurdsson & Phinney 1995), equating the simulated concentration and radial density profile with the observed values. Fig. 8 shows the resulting models for Cetus (obtained for $W_0 = 5$ and $c = 1.20$) and for Tucana (obtained for $W_0 = 1.9$ and $c = 0.73$). In the case of Tucana, the simulated profile and the concentration of the model match the observations reported in Bernard et al. (2009). For the concentration of Cetus, we adopt $c = 1.2$, which best matches our data. We note that the model for Cetus has a relatively high value of W_0, with respect to other dSphs (generally, $W_0 \geq 6$ for globular clusters and $W_0 \lesssim 3$ for dSphs).

In our model, BSSs are generated with a given position, velocity, mass and lifetime. The fundamental differences between COL-BSSs and MT-BSSs are the following:

(i) The distribution of initial positions: the initial positions of MT-BSSs are randomly chosen according to a probability distribution homogeneous in radial distance from the center. This means that MT-BSSs are initially distributed according to an isothermal sphere, since MT-BSSs are expected to follow the same distribution as the primordial binaries (see Mapelli et al. 2004, 2006). (The spherical nature of the dSphs is not conclusively established, but is chosen as a reasonable starting point.) The minimum and the maximum value of the distribution of initial radial distances of MT-BSSs, $r_{\rm min, MT}$ and $r_{\rm max, MT}$ (both defined as three-dimensional quantities), have been tuned in order to find the best-fitting simulation. On the other hand, COL-BSSs are generated only inside r_c (i.e., $r_{\rm min, COL} = 0$ and $r_{\rm max, COL} = r_c$ in all

---

[15] The observed velocity dispersion, v_{obs}, is higher (~ 17 km s^{-1}) for both Cetus (Lewis et al. 2007) and Tucana (Fraternali et al. 2009), but there is evidence that a significant part of it might be due to rotation.

the simulations), the only region were collisions might occur, although collisions are highly unlikely in dSphs (the probability of a three-body interaction in the core of Cetus and Tucana is $\gtrsim 10^5$ times lower than in a moderately dense globular cluster). The initial distribution of COL-BSSs is not necessarily homogeneous in the radial distance, as they are not expected to follow the same distribution as binaries (in our simulations, we assume a constant probability distribution between the center of the cluster and r_c).

(ii) The distribution of initial velocities: the initial velocities of MT-BSSs are drawn from the equilibrium distributions of dSph stars with the same masses as the MT-BSSs. COL-BSSs are assumed to be born with a natal kick (see Sigurdsson et al. 1994). We adopt a kick velocity, $v_{\rm kick}, = 1 - 2\,\sigma_c$. For kick velocities higher than $2\,\sigma_c$ most of COL-BSSs are ejected from the dSph, whereas for kick velocities lower than $1\,\sigma_c$, COL-BSSs are almost indistinguishable from MT-BSSs from a dynamical point of view.

In most of the runs, the masses of the BSSs are assumed to be $m_{\rm BS} = 1.3$ M$_\odot$. We also calculated simulations with $m_{\rm BS} = 0.9, 1.1$ M$_\odot$, but the results are substantially unchanged. Each BSS is evolved for a time t, randomly selected from a homogeneous distribution between $t = 0$ and $t = t_{\rm life}$. The parameter $t_{\rm life}$ is the lifetime of BSSs (see Mapelli et al. 2004). We calculated simulations with $t_{\rm life} = 2$ and 4 Gyr (4 Gyr is the age inferred from the derived SFH).

4.2. Comparison with observations

Tables 2 and 3 show the parameters of the simulations and report also the fraction η of COL-BSSs present in each run ($\eta \equiv N_{\rm COL-BSS}/(N_{\rm COL-BSS} + N_{\rm MT-BSS})$, where $N_{\rm COL-BSS}$ and $N_{\rm MT-BSS}$ are the number of COL-BSSs and of MT-BSSs, respectively). The results of the χ^2 analysis are also included. For each run (we made 38 runs for Cetus and 37 for Tucana) 10000 BSSs have been simulated. We show three values of the non-reduced χ^2, referring to $N_{\rm BS\_RGB}$ ($\chi^2_{\rm RGB}$, column 8 of Tables 2 and 3), $N_{\rm BS\_SGB}$ ($\chi^2_{\rm SGB}$, column 9) and $N_{\rm BS\_HB}$ ($\chi^2_{\rm HB}$, column 10). Fig. 9 shows the radial distributions of $N_{\rm BS\_RGB}$, $N_{\rm BS\_SGB}$, and $N_{\rm BS\_HB}$ obtained for the best-matching simulations (run C3 and run T7 for Cetus and Tucana, respectively), compared with the observed distributions (the same as in Fig. 5). We stress that only the radial distribution of $N_{\rm BSS}$ comes from the simulations, and it is compared with the observed radial distribution of $N_{\rm RGB}$, $N_{\rm HB}$ and $N_{\rm SGB}$. In fact, the adopted simulation method does not allow to evolve these specific stellar types, but only stars in a given class of mass (e.g., Mapelli et al. 2004). We also remind that the underlying potential of the dSph is analytic and time-independent[16]. The best-matching simulations reproduce well the observed radial distributions of $N_{\rm BS\_RGB}$, $N_{\rm BS\_SGB}$, and $N_{\rm BS\_HB}$. In fact, the values of the minimum non-reduced χ^2 are $\chi^2_{\rm RGB} \lesssim 6$, $\chi^2_{\rm SGB} \lesssim 5$ and $\chi^2_{\rm SGB} \lesssim 4$ for Cetus (run C3) and $\chi^2_{\rm RGB} \lesssim 3$, $\chi^2_{\rm SGB} \lesssim 2$ and $\chi^2_{\rm SGB} \lesssim 2$ for Tucana (runs

---

[16] A fully N-body simulation, which may account for the dynamical and stellar evolution of all the aforementioned populations, would give a much more realistic description of the system, but the computational time for running a complete grid of such simulations is prohibitive even for star clusters, let alone for dwarf spheroidals.
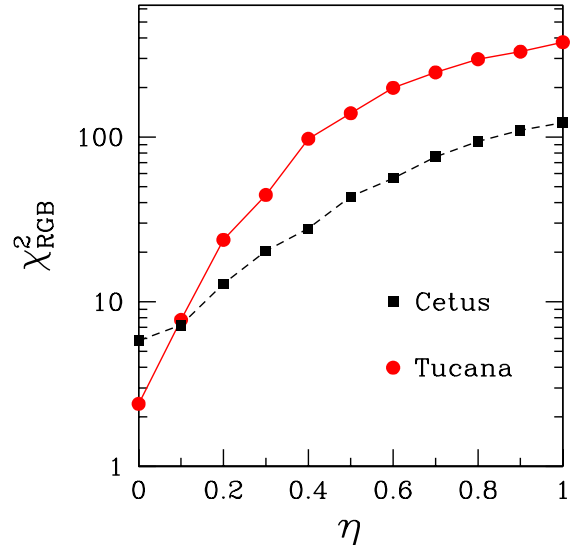

FIG. 10.— $\chi^2_{\rm RGB}$ as a function of the fraction of COL-BSSs (η) for the simulations of Cetus (squares connected by the dashed line) and Tucana (circles connected by the solid line). For each run, only eta was changed, while the other parameters are the same of the best models (C3 and T7 for Cetus and Tucana respectively) and were held constant.

T5, T7, T14, T15, and T16).

Fig 10 shows the behavior of $\chi^2_{\rm RGB}$ (that of $\chi^2_{\rm SGB}$ and of $\chi^2_{\rm HB}$ is very similar, see Tables 2 and 3) as a function of the fraction of COL-BSSs (η). As it was reasonable to expect, adding a population of COL-BSSs significantly reduces the agreement between data and model: for both Cetus and Tucana, only simulations with $\eta < 0.2$ give an acceptable χ^2.

The dependence of the results on the BSSs mass (in the range allowed by the observations) is negligible. This is in agreement with the findings of previous papers (Mapelli et al. 2007, 2009) for BSSs in Draco, Ursa Minor, and Sculptor. The dependence on the lifetime of BSSs is negligible for Cetus (where the runs with $t_{\rm life} = 2$ Gyr are almost equivalent to the runs with $t_{\rm life} = 4$ Gyr) and slightly more important for Tucana (where the runs with $t_{\rm life} = 2$ Gyr have generally lower values of χ^2 with respect to the runs with $t_{\rm life} = 4$ Gyr, but the difference is not statistically significant). Given the range of masses expected for the BSS, suggested by the comparison with stellar tracks, we assume 4 Gyr as fiducial value.

In the case of Cetus, for the best-matching runs $r_{\rm min} \sim 0.0$ and $r_{\rm max} \sim 5\,r_c$, indicating that primordial binaries were initially distributed ranging from the center of the dSph out to (at least) $5\,r_c$. The tidal radius of Cetus (derived from our data) is 24′, i.e., $\sim 15\,r_c$, much larger than $r_{\rm max}$. However, this difference likely does not mean that BSSs do not form beyond $5\,r_c$, but is a consequence of the fact that we do not have data beyond $\approx 4\,r_c$ (furthermore, the coverage of Cetus is not complete even inside $4\,r_c$). In the case of Tucana, for which data are available almost up to the tidal radius, the best-matching value of $r_{\rm max}$ is equal to the tidal radius. Interestingly, the best-matching values of $r_{\rm min}$ for Tucana are all larger than
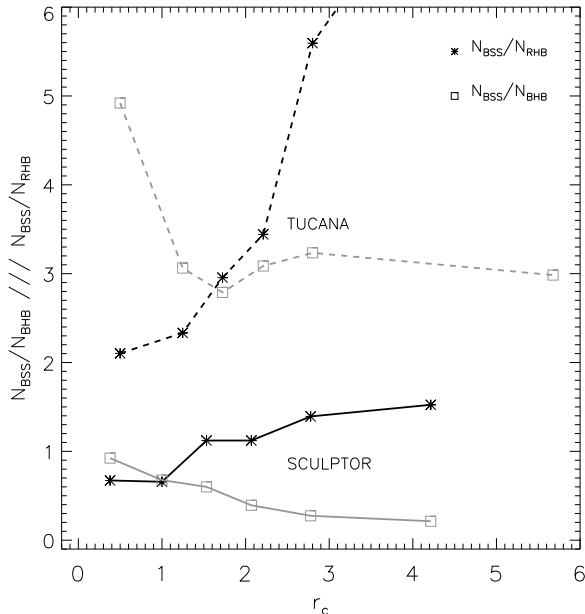
FIG. 11.— The trend with the radial distance of the stellar population ratios N_{BSS}/N_{BHB} and N_{BSS}/N_{RHB} for both Tucana and Sculptor (see text for more details).

FIG. 12.— Ratios as a function of galactocentric distance for different samples of stars. BSSs (left) and HB stars (right) are compared to red (assterisks, dashed line) and blue (open symbols and solid line) RGB stars for Tucana (top) and Cetus (bottom).

one core radius.

In summary, the results of dynamical simulations show that it is possible to explain the observed distribution of BSS candidates, in both Cetus and Tucana, with a MT-BSS population. Any population of COL-BSSs more numerous than the 10% of the total number of BSSs reduces the agreement between data and simulations. This result is not surprising, as basic dynamical calculations tend to exclude the existence of COL-BSSs in dSphs, but it is important to point out that the simulations can almost rule out the unphysical scenario where $> 20\%$ of BSSs are COL-BSSs in both Cetus and Tucana.

5. COMPARISON WITH THE SCULPTOR DSPH

The results discussed in the previous sections provide evidence that the two isolated dwarf galaxies Cetus and Tucana host a significant population of BSSs, whose properties strongly suggest that they are the product of mass exchange in binary systems. We did not find any evidence supporting the hypothesis that part of the objects populating the blue plume are intermediate-age or young MS stars. On the basis of these findings, it appears that both Cetus and Tucana are similar to Ursa Minor, Draco (Mapelli et al. 2007), and Sculptor (Mapelli et al. 2009). In the following, we first focus on the comparison of Tucana and Sculptor, two dwarfs which show close similarities in terms of their SFH and present-day stellar content.

Sculptor is a well established case of a dSph galaxy hosting two different old populations. Majewski et al. (1999) first noted evidence of two RGB bumps in Sculptor. Tolstoy et al. (2004) presented a photometric and spectroscopic (235 RGB stars) investigation of this galaxy, showing the presence of strong radial gradients and two stellar populations with different kinematic and chemical properties. Moreover, the radial distributions of the red and blue HB components are correlated
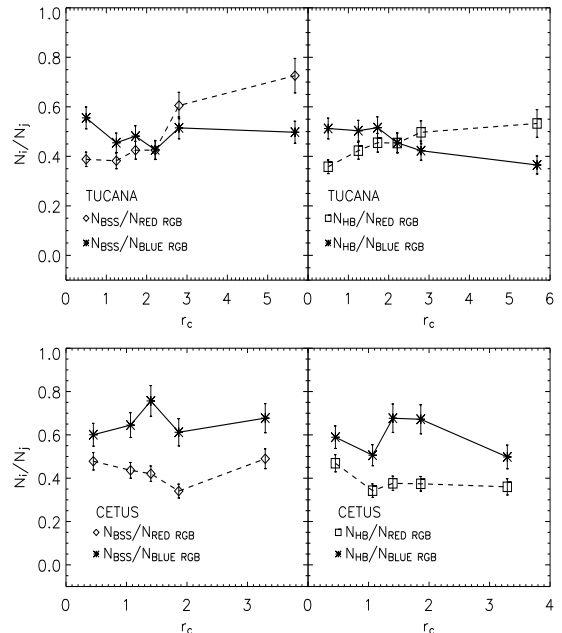
with the properties of the RGB stars, suggesting that red stars are more centrally concentrated, more metal-rich, and have a higher velocity dispersion, while the blue component has a broader distribution, lower metallicity, and a smaller velocity dispersion.

Bernard et al. (2008) showed the first evidence of stellar radial gradients in Tucana; after dividing both the HB and the RGB into red and blue components, the number of stars belonging to the red components decreases faster than the corresponding blue sequence with increasing galaxy radius. Moreover, the analysis of the properties of RR Lyrae variables stars (Bernard et al. 2009), the SFH (Monelli et al. 2010c), and the double RGB bump (Monelli et al. 2010a) strongly support the coexistence of two old (> 10 Gyr) populations in Tucana, with slightly different ages, metallicities, and spatial distributions.

Figure 11 compares the ratio of the number of BSSs versus red (asterisks) and blue (squares) HB stars as a function of galactocentric radius for the two galaxies. The values for Sculptor are taken from Table 2 of Mapelli et al. (2009). Interestingly, in both cases the BSSs are more centrally concentrated than the blue component of the HB, and less concentrated than the red component. We note also that, for each galaxy, the two curves cross at a similar galactocentric distance, $\approx 1 - 1.6$ r_c. In the case of Tucana, this trend is confirmed also for the BSSs and the HB stars when compared to red and blue RGB stars (Figure 12, top left and top right, respectively). Therefore, if we compare the global N_{BSS}/N_{HB} ratio in Figure 5 with Figure 11 and Figure 12 (top panels), it can be inferred that the radial trends of the BSSs are indeed driven by the fast decrease of the red HB stars in the central regions, associated with the younger, more metal-rich component, while the increase at larger radii is driven by the more homogeneously distributed

TABLE 2
PARAMETERS AND VALUES OF χ^2 FOR THE SIMULATIONS OF CETUS.

Case [a]	$r_{\rm min, MT}/r_{\rm c}$ [b]	$r_{\rm max, MT}/r_{\rm c}$ [b]	$m_{\rm BSS}/M_\odot$ [c]	$t_{\rm life}/$ Gyr [d]	$v_{\rm kick}/\sigma_{\rm c}$ [e]	η [f]	$\chi^2_{\rm RGB}$ [g]	$\chi^2_{\rm SGB}$ [g]	$\chi^2_{\rm HB}$ [g]
C1	0.0	5.0	0.9	4	–	0	7.7	6.5	4.7
C2	0.0	5.0	1.1	4	–	0	9.5	8.1	5.8
C3	**0.0**	**5.0**	**1.3**	**4**	–	**0**	**5.8**	**4.9**	**3.5**
C4	0.1	5.0	1.3	4	–	0	8.3	7.0	5.0
C5	0.2	5.0	1.3	4	–	0	7.3	6.2	4.5
C6	0.3	5.0	1.3	4	–	0	10	8.7	6.2
C7	0.4	5.0	1.3	4	–	0	14	12	8.5
C8	0.5	5.0	1.3	4	–	0	19	16	12
C9	1.0	5.0	1.3	4	–	0	51	42	31
C10	0.0	5.0	0.9	2	–	0	6.7	5.6	4.1
C11	0.0	5.0	1.1	2	–	0	7.2	6.1	4.4
C12	0.0	5.0	1.3	2	–	0	9.8	8.3	5.9
C13	0.1	5.0	1.3	2	–	0	9.0	7.6	5.4
C14	0.2	5.0	1.3	2	–	0	7.0	5.9	4.2
C15	0.3	5.0	1.3	2	–	0	7.5	6.3	4.6
C16	0.4	5.0	1.3	2	–	0	12	10	7.5
C17	0.5	5.0	1.3	2	–	0	20	17	12
C18	1.0	5.0	1.3	2	–	0	50	41	30
C19	0.0	4.0	1.3	4	–	0	10	8.7	6.2
C20	0.2	4.0	1.3	4	–	0	9.4	7.8	5.5
C21	0.5	4.0	1.3	4	–	0	7.9	6.7	4.8
C22	1.0	4.0	1.3	4	–	0	41	34	25
C23	0.0	6.0	1.3	4	–	0	13	11	7.7
C24	0.2	6.0	1.3	4	–	0	16	13	9.1
C25	0.5	6.0	1.3	4	–	0	26	22	16
C26	1.0	6.0	1.3	4	–	0	77	64	46
C27	0.0	5.0	1.3	4	1	0.1	7.2	6.0	4.3
C28	0.0	5.0	1.3	4	1	0.2	13	11	7.8
C29	0.0	5.0	1.3	4	1	0.3	20	17	12
C30	0.0	5.0	1.3	4	1	0.4	28	23	16
C31	0.0	5.0	1.3	4	1	0.5	43	36	26
C32	0.0	5.0	1.3	4	1	0.6	56	47	33
C33	0.0	5.0	1.3	4	1	0.7	76	63	45
C34	0.0	5.0	1.3	4	1	0.8	94	78	56
C35	0.0	5.0	1.3	4	1	0.9	110	91	65
C36	–	–	1.3	4	1	1.0	122	101	72
C37	0.0	5.0	1.3	4	2	0.1	9.4	7.9	5.7
C38	0.0	5.0	1.3	4	2	0.2	14	12	8.3

[a] Identifier of the run (for each run, 10000 BSSs have been simulated).
[b] $r_{\rm min, MT}$ and $r_{\rm max, MT}$ are the minimum and the maximum three-dimensional radius within which MT-BSSs are generated in the simulations. The minimum and the maximum three-dimensional radius within which COL-BSSs are generated in the simulations are not listed in the Table, because they are the same in all the simulations (i.e., $r_{\rm min, COL} = 0$ and $r_{\rm max, COL} = r_{\rm c}$, respectively).
[c] Mass of a simulated BSS. In the simulations, $m_{\rm BSS}$ is the same for MT-BSSs and COL-BSSs.
[d] Lifetime of a simulated BSS. In the simulations, $t_{\rm life}$ is the same for MT-BSSs and COL-BSSs.
[e] Kick velocity for COL-BSSs.
[f] Fraction of simulated COL-BSSs with respect to the total population of BSSs.
[g] $\chi^2_{\rm RGB}$, $\chi^2_{\rm SGB}$ and $\chi^2_{\rm HB}$ are the non-reduced χ^2 of the simulated $N_{\rm BS\_RGB}$, $N_{\rm BS\_SGB}$ and $N_{\rm BS\_HB}$.

bluest stars. This means that the peculiar radial trend of the candidate BSSs when they are normalized to the HB stars is not due to a peculiar distribution of these objects inside the galaxy but only to the existence of a significant metallicity gradient in Tucana, a gradient that is well traced by both the red and blue HB stellar populations.

The similarities between these two galaxies are particularly intriguing because of the remarkably different environmental conditions: Tucana spent most of its life in isolation, while Sculptor is a close satellite of the Milky Way. If all the BSSs are descendants of primordial binaries, this suggests that the different environments of the two galaxies did not alter their binary distributions.

In contrast, Figure 12 (bottom panels) shows that the properties of different stellar samples in Cetus appear more homogeneous. This would be in agreement with other findings, as the properties of the RR Lyrae variable stars and of the RGB bump, which indicate a single

dominant population characterized by a more uniform distribution of ages and metallicities.

Interesting features appear when comparing the distribution of the BSSs with those of the red and blue stars of both the RGB and HB. We defined these samples as follows. The region selecting the RGB stars was simply split in two, similarly to what has been done for the analysis of the RGB bump in Monelli et al. (2010a). The red and blue HB are defined considering only the stars redder than $m_{F475W} - m_{F814W} > 0.99$ and bluer than $m_{F475W} - m_{F814W} < 0.46$ in the HB region, therefore mostly avoiding the RR Lyrae instability strip. Figure 13 compares the distributions of these four samples with the BSSs for both Tucana and Cetus. In the case of Cetus, we find that the BSSs are significantly less concentrated than the red HB and more concentrated than the blue HB, while they more closely follow the distributions of both of the RGB components. In the case of Tucana, the BSSs closely follow the distributions of both blue

TABLE 3
PARAMETERS AND VALUES OF χ^2 FOR THE SIMULATIONS OF TUCANA.

Case [a]	$r_{\mathrm{min,MT}}/r_{\mathrm{c}}$ [b]	$r_{\mathrm{max,MT}}/r_{\mathrm{c}}$ [b]	$m_{\mathrm{BSS}}/M_{\odot}$ [c]	$t_{\mathrm{life}}/$ Gyr [d]	$v_{\mathrm{kick}}/\sigma_{\mathrm{c}}$ [e]	η [f]	χ^2_{RGB} [g]	χ^2_{SGB} [g]	χ^2_{HB} [g]
T1	0.0	5.4	1.3	4	0	–	101	78	60
T2	0.5	5.4	1.3	4	0	–	51	40	30
T3	1.0	5.4	1.3	4	0	–	21	17	12
T4	1.5	5.4	1.3	4	0	–	5.7	4.6	3.4
T5	1.7	5.4	0.9	4	0	–	2.6	2.1	1.6
T6	1.7	5.4	1.1	4	0	–	3.2	2.6	1.9
T7	**1.7**	**5.4**	**1.3**	**4**	**0**	**–**	**2.4**	**1.9**	**1.5**
T8	2.0	5.4	1.3	4	0	–	7.7	6.1	4.8
T9	2.5	5.4	1.3	4	0	–	18	14	11
T10	0.0	5.4	1.3	2	0	–	106	83	63
T11	0.5	5.4	1.3	2	0	–	55	43	33
T12	1.0	5.4	1.3	2	0	–	23	18	14
T13	1.5	5.4	1.3	2	0	–	2.5	2.1	1.5
T14	1.7	5.4	0.9	2	0	–	2.3	1.8	1.4
T15	1.7	5.4	1.1	2	0	–	1.9	1.5	1.1
T16	1.7	5.4	1.3	2	0	–	1.6	1.3	0.95
T17	2.0	5.4	1.3	2	0	–	4.8	3.7	2.9
T18	2.5	5.4	1.3	2	0	–	16	13	9.8
T19	0.0	4.0	1.3	4	0	–	139	109	83
T20	0.5	4.0	1.3	4	0	–	83	65	49
T21	1.0	4.0	1.3	4	0	–	41	32	24
T22	1.5	4.0	1.3	4	0	–	15	12	8.6
T23	1.7	4.0	1.3	4	0	–	5.5	4.5	3.3
T24	2.0	4.0	1.3	4	0	–	6.3	4.9	3.8
T25	2.5	4.0	1.3	4	0	–	11	8.7	6.7
T26	1.7	5.4	1.3	4	1	0.1	7.8	6.0	4.5
T27	1.7	5.4	1.3	4	1	0.2	24	18	14
T28	1.7	5.4	1.3	4	1	0.3	45	34	26
T29	1.7	5.4	1.3	4	1	0.4	98	76	58
T30	1.7	5.4	1.3	4	1	0.5	140	109	84
T31	1.7	5.4	1.3	4	1	0.6	199	156	120
T32	1.7	5.4	1.3	4	1	0.7	247	195	149
T33	1.7	5.4	1.3	4	1	0.8	297	236	180
T34	1.7	5.4	1.3	4	1	0.9	330	262	200
T35	–	–	1.3	4	1	1.0	377	301	229
T36	1.7	5.4	1.3	4	2	0.1	5.8	4.5	3.3
T37	1.7	5.4	1.3	4	2	0.2	24	18	15

[a] Identifier of the run (for each run, 10000 BSSs have been simulated).
[b] $r_{\mathrm{min,MT}}$ and $r_{\mathrm{max,MT}}$ are the minimum and the maximum three-dimensional radius within which MT-BSSs are generated in the simulations. The minimum and the maximum three-dimensional radius within which COL-BSSs are generated in the simulations are not listed in the Table, because they are the same in all the simulations (i.e., $r_{\mathrm{min,COL}} = 0$ and $r_{\mathrm{max,COL}} = r_{\mathrm{c}}$, respectively).
[c] Mass of a simulated BSS. In the simulations, m_{BSS} is the same for MT-BSSs and COL-BSSs.
[d] Lifetime of a simulated BSS. In the simulations, t_{life} is the same for MT-BSSs and COL-BSSs.
[e] Kick velocity for COL-BSSs.
[f] Fraction of simulated COL-BSSs with respect to the total population of BSSs.
[g] χ^2_{RGB}, χ^2_{SGB} and χ^2_{HB} are the non-reduced χ^2 of the simulated $N_{\mathrm{BS\_RGB}}$, $N_{\mathrm{BS\_SGB}}$ and $N_{\mathrm{BS\_HB}}$.

components (possibly more concentrated in the central regions), while they are significantly less concentrated than the red sequences.

We have demonstrated that the populations of BSS candidates in Tucana and Cetus are consistent with all predictions of creation from MT-BSSs. In fact, it would be unprecedented to have a truncation in star formation without an associated population of MT-BSSs. Unfortunately, our limited knowledge of the evolution of binary stellar systems prevents us from making accurate predictions of the expected numbers of MT-BSSs. In sum, we expect to see MT-BSSs in dSph galaxies, and we detect them with consistent properties. The remaining question is whether some fraction of the BSS candidates could still be due to newly formed MS stars. The inconsistency with the age-metallicity relationship could be due to infall of a gas cloud with a low metallicity coincident with that of the main population which then produces subsequent star formation. However, the truncation at luminosities

corresponding to twice the TO mass implies a second unlikely coincidence if some of the BSS candidates were true MS stars. While very difficult to rule out such a scenario completely, it is clear that newly formed MS stars are not necessary to explain all of the observations.

6. SUMMARY AND CONCLUSION

In this paper, we have presented the analysis of candidate BSSs in two isolated dSphs in the periphery of the Local Group, Cetus and Tucana. Deep HST/ACS data allowed us to identify 940 and 1214 BSS candidates in Cetus and Tucana, respectively. Different indicators suggest that these are true BSSs; and, thus, there are no young main sequence stars in either galaxy. The first evidence comes from the SFH we derived for both objects (Monelli et al. 2010b,c). Not allowing for the presence of BSSs, then a small population of relatively young (3 to 5 Gyr old) stars is detected, with metallicities similar to the oldest most metal-poor stars, and thus, much lower than expected from the age-metallicity relation of
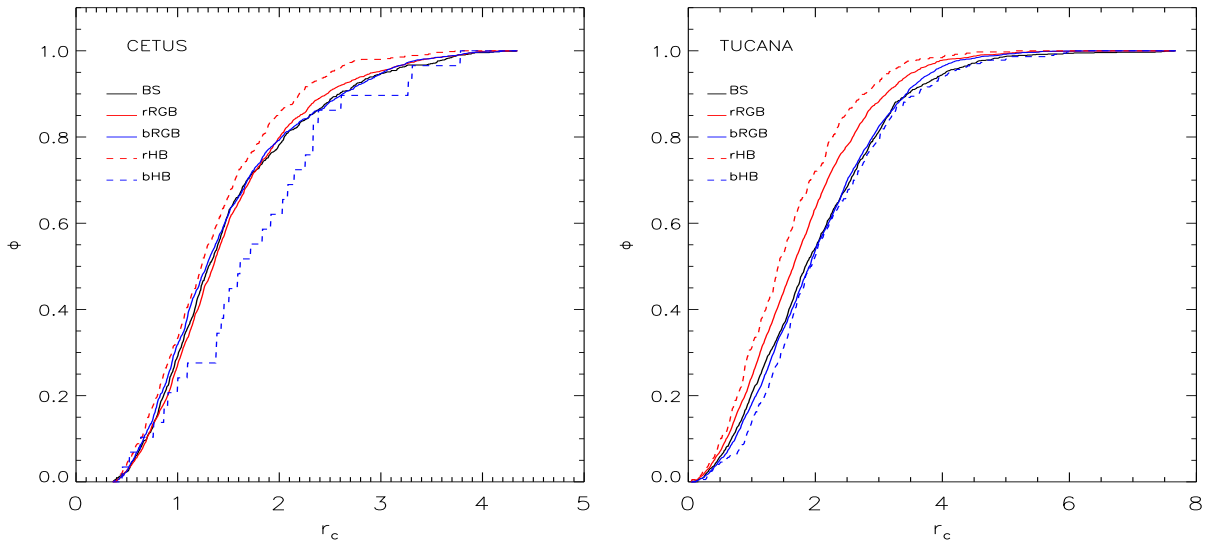
FIG. 13.— Normalized cumulative distributions for the samples of BSSs (black solid line) compared to red and blue RGB stars (red and blue solid lines), and red and blue HB stars (red and blue dashed). In the Case of Cetus (left panel), the BSSs are more concentrated than the blue HB stars, and less concentrated than the red HB stars. In the case of Tucana (right panel), the BSSs are less concentrated than both the red RGB and HB samples, while they are marginally more concentrated than the blue components.

the dominant population. The comparison with stellar tracks presented in this paper suggests that the BSSs have typical masses $> 1 M_\odot$, and smaller than $\sim 1.5 M_\odot$, in agreement with the fact that the maximum expected mass of a BSS is twice the mass presently evolving at the TO ($\sim 0.8 M_\odot$). Moreover, the limited spread in metallicity found for the BSS populations, perfectly in agreement with that of turn-off and subgiant stars, suggests that the use of stellar evolution models for single stars does not introduce strong biases in the analysis.

The analysis of the luminosity functions and radial distributions support the BSS interpretation. On one hand, we showed that the luminosity function does not change as a function of radius, and in particular the brightest (youngest) stars do not appear more centrally concentrated, as one would expect from a young main sequence. On the other hand, the radial profiles do not show any central peak, as observed in globular clusters due to COL-BSS stars or as it would be in the case of a young component.

Thus, the present analysis also suggests that the BSSs in Cetus and Tucana formed from primordial binaries and, as in the case of other dSphs, COL-BSSs are unlikely to form. This conclusion is strongly supported by the dynamical simulations we performed, taking into account the properties of the dwarfs under scrutiny. These simulations indicate that the observed BSS distributions are well reproduced when only MT-BSSs are taken into account, while the fit worsens when even a small number of COL-BSSs ($\sim 10\%$) is included in the dynamical simulation.

We can therefore safely conclude that it is highly likely that Cetus and Tucana host a genuine population of BSS stars, and we confirm the conclusions presented in previous studies that both galaxies did not experience any star formation episodes in the last 8 Gyr. It is particularly interesting that the positions of Cetus and Tucana in the F_{BS} vs. M_V plane fit very well in the relation presented by Momany et al. (2007). This, in turn, could be a powerful instrument to identify young main sequence stars in resolved spheroidal galaxies, discriminating from systems with only old populations from those also hosting younger stars.

REFERENCES

Bailyn, C. D. 1995, ARA&A, 33, 133
Bailyn, C. D., & Pinsonneault, M. H. 1995, ApJ, 439, 705
Bernard E. J., et al. 2008, ApJ, 678, L21
Bernard E. J, et al. 2009, ApJ, 699, 1742
Bono, G., Caputo, F., Santolamazza, P., Cassisi, S., & Piersimoni, A. 1997, AJ, 113, 2209
Carney, B.W., Latham, D.W., & Laird, J.B. 2005, AJ, 129, 466
Castellani, V., & Degl'Innocenti, S. 1995, A&A, 298, 827
Ferraro, F. R., et al. 2009, Nature, 462, 1028
Fraternali, F., Tolstoy, E., Irwin, M. J., Cole, A. A. 2009, A&A, 499, 121
Gilliland, R.L., Bono, G., Edmonds, P.D., Caputo, F., Cassisi, S., Petro, L.D., Saha, A., & Shara, M.M. 1998, ApJ, 507, 818
Hidalgo, S. L., et al. 2011, ApJ, 730, 14

Hills, J.G., & Day, C.A. 1976, ApL, 17, 87

Lee, M. G., et al. 2003, AJ, 126, 2840

Liu, G.Q., Deng, L., Chávez, M., Bertone, E., Davo, A.H., Mata-Chávez, M.D. 2008, MNRAS, 390, 665

Lewis, G. F., Ibata, R. A., Chapman, S. C., McConnachie, A., Irwin, M. J., Tolstoy, E., Tanvir, N. R. 2007, MNRAS, 375, 1364

Mapelli, M., Sigurdsson, S., Colpi, M., Ferraro, F. R., Possenti, A., Rood, R. T., Sills, A., & Beccari, G. 2004, ApJ, 605, L29

Mapelli, M., Sigurdsson, S., Ferraro, F. R., Colpi, M., Possenti, A., & Lanzoni, B. 2006, MNRAS, 373, 361

Mapelli, M., Ripamonti E., Tolstoy E., Sigurdsson S., Irwin M. J., & Battaglia G., 2007, MNRAS, 380, 112

Mapelli, M., Ripamonti, E., Battaglia, G., Tolstoy, E., Irwin, M. J., Moore, B., & Sigurdsson, S. 2009, MNRAS, 396, 1771

Mateo, M., Nemec, J., Irwin, M., & McMahon, R. 1991, AJ, 101, 892

Majewski, S. R., Siegel, M. H., Patterson, R. J., & Rood, R. T. 1999, ApJ, 520, L33

McConnachie, A.W. & Irwin, M.J., 2006, MNRAS, 365, 1263

McCrea, W.H. 1964, MNRAS, 128, 147

Momany, Y., Held, E. V., Saviane, I., Zaggia, S., Rizzi, L., & Gullieuszik, M. 2007, A&A, 468, 973

Monelli, M., Cassisi, S., Bernard, E. J., Hidalgo, S. L., Aparicio, A., Gallart, C., & Skillman, E. D. 2010, ApJ, 718, 707

Monelli, M., et al. 2010, ApJ, 720, 1225

Monelli, M., et al. 2010, ApJ, 722, 1864

Monkman, E., Sills, A., Howell, J., Guhathakurta, P., de Angeli, F., & Beccari, G. 2006, ApJ, 650, 195

Pietrinferni, A., Cassisi, S., Salaris, M., Castelli, F. 2004, ApJ, 612, 168

Piotto, G., De Angeli, F., King, I.R., et al. 2004, ApJ, 604, L109

Sandage, A. R. 1953, AJ, 58, 61

Saviane, I., Held, E. V., & Piotto, G. 1996, A&A, 315, 40

Sigurdsson, S., Davies, M. B., Bolte, M. 1994, ApJ, 431, L115

Sigurdsson, S., Phinney, E. S. 1995, ApJS, 99, 609

Sills, A., Karakas, A., & Lattanzio, J. 2009, ApJ, 692, 1411

Sirianni, M. et al. 2005, PASP, 117, 1049

Stetson, P. B. 1994, PASP, 106, 250

Stetson, P. B., Hesser, J. E., & Smecker-Hane, T. A. 1998, PASP, 110, 533

Stryker, L. L. 1993, PASP, 105, 1081

Tolstoy, E., et al. 2004, ApJ, 617, L119